Review of Scientific Instruments

Design and operation of a scanning electrochemical microscope for imaging with continuous line probes

Cite as: Rev. Sci. Instrum. **90**, 083702 (2019); https://doi.org/10.1063/1.5095951
Submitted: 13 March 2019 . Accepted: 18 July 2019 . Published Online: 20 August 2019

Anna E. Dorfi, Han-wen Kuo, Vera Smirnova, John Wright, and Daniel V. Esposito

Review of Scientific Instruments ARTICLE scitation.org/journal/rsi

Design and operation of a scanning electrochemical microscope for imaging with continuous line probes

Cite as: Rev. Sci. Instrum. 90, 083702 (2019); doi: 10.1063/1.5095951
Submitted: 13 March 2019 • Accepted: 18 July 2019 •
Published Online: 20 August 2019

Anna E. Dorfi,[1] Han-wen Kuo,[2] Vera Smirnova,[1] John Wright,[2,a)] and Daniel V. Esposito[1,a)]

AFFILIATIONS

[1] Department of Chemical Engineering, Columbia Electrochemical Energy Center, Lenfest Center for Sustainable Energy, Columbia University in the City of New York, New York, New York 10027, USA

[2] Department of Electrical Engineering, Data Science Institute, Columbia University in the City of New York, New York, New York 10027, USA

[a)] **Authors to whom correspondence should be addressed:** jw2966@columbia.edu and de2300@columbia.edu

ABSTRACT

This article describes a home-built scanning electrochemical microscope capable of achieving high areal imaging rates through the use of continuous line probes (CLPs) and compressed sensing (CS) image reconstruction. The CLP is a nonlocal probe consisting of a band electrode, where the achievable spatial resolution is set by the thickness of the band and the achievable imaging rate is largely determined by its width. A combination of linear and rotational motors allows for CLP scanning at different angles over areas up to 25 cm^2 to generate the raw signal necessary to reconstruct the desired electrochemical image using CS signal analysis algorithms. Herein, we provide detailed descriptions of CLP fabrication, microscope design, and the procedures used to carry out scanning electrochemical microscopy imaging with CLPs. In order to illustrate the basic operating procedures for the microscope, line scans and images measured in the substrate generation-probe-collection mode for flat samples containing platinum disk electrodes are presented. These exemplary measurements illustrate methods for calibrating the positioning system, positioning and cleaning the CLP, and verifying proper positioning/probe sensitivity along its length.

I. INTRODUCTION

Scanning electrochemical microscopy (SECM) is a powerful scanning probe microscopy (SPM) imaging method used for evaluating the chemical and physical properties of materials at microscopic and nanoscopic length scales.[1–5] The vast majority of SECM measurements performed to date have used conventional ultramicroelectrode (UME) probes, which typically consist of a metallic wire sealed in an insulating glass sheath. During operation, the electrochemical interaction between this UME "point probe" and the sample is recorded in a point-by-point sensing scheme as the UME is scanned across an area of interest. A major shortcoming of conventional point probes is that they require very long scan times to image large sample areas with high resolution.[6,7] In general, long scan times result in low throughput and can lead to unwanted changes in the sample or probe.

Previous research efforts have attempted to overcome the trade-off between resolution and areal imaging rates through a variety of approaches that have involved modifications to SECM hardware,[1,8–12] the use of advanced probe geometries,[13–16] and/or post-measurement image processing to correct for blurriness and artifacts associated with fast scan speeds.[13,15–18] For example, the development of scanning droplet cells for scanning electrochemical cell microscopy (SECCM), combined with the use of more efficient spiral scan patterns, has resulted in substantial increases in areal imaging rates, thanks to their ability to utilize high scan rates without being limited by convection.[2,3,19–21] Alongside instrument development, the use of innovative probe configurations and geometries has emerged as a promising approach to increase SECM imaging rates.[13,14,22–24] For example, multiple studies have demonstrated the use of individually addressable submicrometer electrodes for large area imaging.[13,15] Lesch *et al.* combined the idea of using a linear

array of microelectrodes with polymeric thin films to create soft, flexible probes capable of imaging large sample areas, even for tilted and curved surfaces.[13,14,25] Yet, the resolution of these probes remains limited by the lateral spacing between the point probes embedded within the array. Additionally, fabrication of these probes is nontrivial, and more complex electronics (e.g., multiplexer or multichannel potentiostat) are required to record the signals from the individually addressable electroactive elements.

Recently, we have demonstrated an alternate approach to increasing SECM imaging rates by using a continuous line probe (CLP) consisting of a high aspect ratio band electrode sealed between two insulating sheets.[22] In principle, the CLP can achieve high imaging rates by sensing probe/substrate interactions everywhere along its length while simultaneously achieving high spatial resolution that is set by the thickness of the band electrode. By performing multiple CLP scans across a region of interest at different substrate scan angles, sufficient information can be obtained to reconstruct a 2D SECM image. A complication of SECM imaging with a CLP (CLP-SECM) is that the nonlocal nature of the CLP requires advanced signal analysis methods to reconstruct images from the convoluted information contained in the raw CLP scans. Fortunately, this task can be efficiently achieved using modern compressed sensing (CS) reconstruction methods.[17,18]

Our previous study described the basic principles of CLP-SECM imaging with CS image reconstruction, but the quality and areal imaging rates demonstrated in that work were limited by the CLPs and the microscope setup employed in that study.[22] Specifically, those first demonstrations involved tedious probe positioning, sample rotation, probe cleaning, and data acquisition procedures that increased imaging times and introduced unnecessary human errors into the measurement scheme. In this paper, we describe a custom-built programmable scanning electrochemical microscope setup for CLP-SECM imaging that can overcome these limitations. The advantages of this new instrument include its ability to perform programmable rotational movements with simple hardware and probe design, allowing for streamlined data acquisition of electrochemical data. Herein, we first describe the procedures for fabricating and characterizing the CLP used in this study before detailing the system design and key microscope components. Subsequently, the communication and control of the hardware is explained and example measurements from the instrument are presented.

II. DESIGN AND OPERATING PRINCIPLES OF CLP-SECM

A. Microscope design and operation

Figure 1 contains a simple block diagram showing the key components of our microscope and how they are configured with respect to each other. The overall design and many of the key components of this microscope share many similarities with the conventional SECM instruments, which have been described in detail in previous publications.[5,26,27] The common SECM components include X, Y, and Z positioners for precise control over the probe position and a bipotentiostat to control the applied potential of the probe and

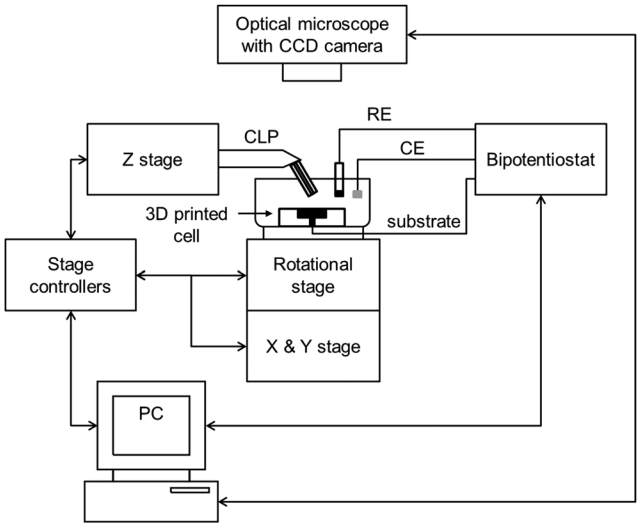

FIG. 1. A schematic of the scanning electrochemical microscope setup with rotational and linear programmable positioners for use with a continuous line probe (CLP).

substrate. A key difference is that the SECM instrument in Fig. 1 is specially designed to carry out imaging with CLPs thanks to the integration of a programmable, high precision rotational positioner that rotates the sample stage in between line scan measurements. The rotational positioner is stacked on top of the linear encoded programmable X and Y positioners, which collectively form the sample stage. An electrochemical cell containing the sample to be imaged is mounted on top of this stage and viewed from above by a CCD camera. A programmable Z positioner, independently secured to the microscope platform, possesses a mounting bracket for the CLP and serves the purpose of raising and lowering the CLP with respect to the sample to be imaged. The X, Y, Z, and rotational (R) positioners are connected to a common controller/power supply unit. The CCD camera, positioner electronics, and bipotentiostat all interface with a personal computer (PC). In Subsections II A 1–II A 3, more details are provided about the design and characteristics of the CLPs, the electrochemical cell, and the positioning system.

1. Continuous line probes (CLPs)

A CLP is typically composed of three layers: an insulating substrate, an electroactive layer, and a thin insulating layer.[22] As shown in Fig. 2(a), the electroactive sensing element is sandwiched between the two insulating layers. The thicker of the two insulating layers serves as the probe substrate, while the thinner insulating layer serves as a spacer between the electroactive layer and the sample during imaging that sets the average probe-substrate separation distance, d_m. The thickness of the electroactive layer, t_E, sets the imaging resolution. The CLP also simultaneously senses features along the width, w, of the probe. In contrast, an ultramicroelectrode (UME), or "point-probe," typically consists of a metal wire that has been sealed in glass and polished at the end to obtain an exposed disk-shaped sensing element that is surrounded by a glass ring. The

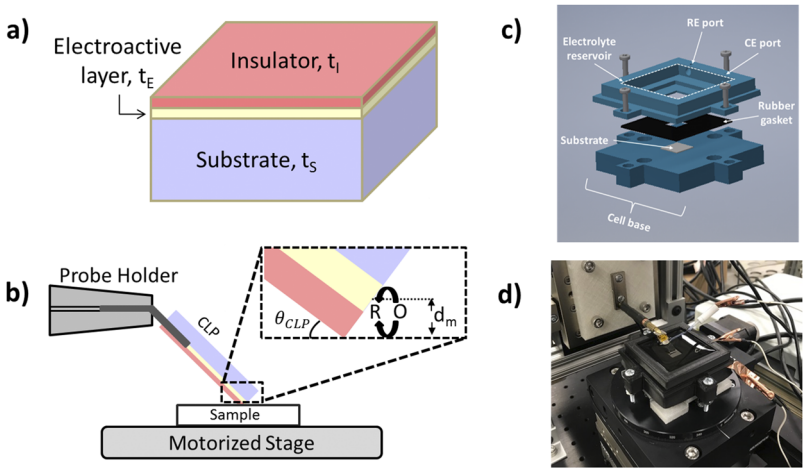

FIG. 2. (a) A schematic 3D view of the different layers of a continuous line probe (CLP), including the insulating top layer, the electroactive layer, and the substrate layer. Layer thicknesses are not drawn to scale. (b) Schematic side-view of a CLP mounted on a probe holder and placed in contact with the sample to be imaged. The inset shows a close-up of the point of contact between the CLP and sample. (c) Exploded-view computer aided design (CAD) drawing of the custom electrochemical cell used in this study. (d) Photograph of the electrochemical cell mounted on the motorized positioning stage with the CLP positioned in the electrolyte for imaging.

spatial resolution that can be achieved by such a probe is limited by the diameter ($2{\cdot}r_0$) of the exposed metal disk electrode. Table I shows a visual comparison of these two probe geometries.

During imaging, the CLP is mounted onto a probe holder attached to the Z-positioner and positioned such that the thinner insulating layer comes in contact with the sample to be imaged [Fig. 2(b)]. The thickness of the thin insulating layer, t_I, combined with the CLP mounting angle with respect to the sample θ_{CLP}, determines the average separation distance between the sample and the electroactive layer [Fig. 2(b), inset]. This average separation thickness d_m is calculated using the following equation:

$$d_m = \left(\frac{t_E}{2} + t_I\right)\sin(90^\circ - \theta_{CLP}). \quad (1)$$

In general, t_I should be similar to the thickness of the electroactive layer t_E in order to ensure that significant positive/negative feedback will be observed during SECM imaging with the CLP. The thickness of the electroactive layer t_E sets the imaging resolution.

2. Electrochemical cell

The SECM measurements were performed in a custom low-profile cell that was designed using engineering design software and made from polylactic acid (PLA) using a 3D printer (MakerGear M3-ID). The computer aided design (CAD) files for this cell have been made freely available on the website www.echem.io, and a 3D rendering can be seen in Fig. 2(c). The cell consists of a base that connects directly to the rotational stage and a top frame component that holds the electrolyte and attaches to the base. When assembling the cell, the sample to be imaged is clamped between the cell base and the frame using bolts and a rectangular rubber gasket to form a liquid-tight seal between the sample and the frame while securely fastening all components to the rotational stage. The front side of the sample is exposed to the electrolyte through a square hole in the bottom of the upper frame component of the cell. Figure 2(d) contains a photograph showing the fully assembled cell mounted on the microscope stage during SECM measurements.

TABLE I. Side-by-side comparison of probe geometries and key features of SECM performed using a continuous line probe (CLP-SECM) and a conventional ultramicroelectrode (UME).

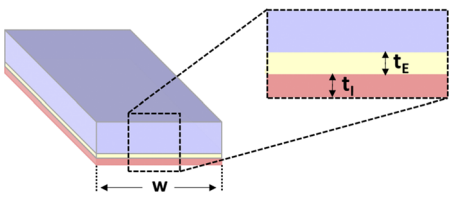

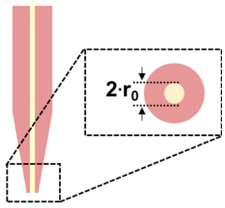

	CLP-SECM	Conventional SECM
Resolution	Set by the electroactive layer thickness, t_E	Set by the disk diameter, $2{\cdot}r_0$
Applications	Large sample areas with low density of features and few feature types	Small sample areas with high density of features and/or many feature types
Fabrication	Lamination, physical vapor deposition, chemical vapor deposition	Pipette puller, wire etching methods

3. Linear and rotational positioners

The X, Y, and Z translational positioners can travel a maximum distance of 50 mm at a maximum velocity of 20 mm s^{-1}. The X and Y programmable positioners (Thorlabs, LNR50SE/M) are optically encoded and can achieve a minimum repeatable positional accuracy of 0.1 μm. The Z positioner (Thorlabs, LNR50S/M) possesses the same specifications as the X and Y stages except that it is not equipped with an optical encoder, having a minimum repeatable positional accuracy of 1 μm. The lower Z-position accuracy is permissible for CLP-SECM imaging since imaging occurs with the CLP in direct contact with the sample such that slight overshoot of the Z-position of the CLP has very little impact on the average probe/substrate separation distance. Rotation of the electrochemical cell is carried out using a rotational stage (Thorlabs, NR360S/M) that travels 360° with a positional accuracy of 5 arc min (≈0.083°). As shown in Fig. 1, the rotational, X, and Y positioners are stacked on top of each other to form the scanning stage upon which the electrochemical cell is mounted. Benchtop controllers (3 channels and 1 channel) are employed for controlling the positioners.

B. Communication and control schemes

The overall communication and control scheme for operation of the CLP-SECM is shown in the process control flow diagram provided in Fig. 3. The control scheme was implemented through LabVIEW, which served as the user interface and platform to coordinate execution of user specified scanning conditions through the bipotentiostat and X, Y, Z, and rotational positioners. Beginning in the lower left corner of Fig. 3, the operator must first enter the desired preconditioning and imaging parameters into the LabVIEW user interface. These include the applied potential for the probe and sample substrate, the coordinates of the center of the sample stage, the CLP scan rate, the scan distance, the probe Z position, the angular position of the substrate, and the total number of scans ***N***. Next, the operator starts the imaging program, which successively executes the three sub-blocks labeled in Fig. 3: (i) probe positioning and conditioning, (ii) execution of a single CLP scan, and (iii) repositioning of the CLP for the following scan. Upon completion of the ***N***th scan, the program ends and the recorded electrochemical data are used for postimage processing and CS image reconstruction. In Subsections II B 1–II B 5, additional details are provided about the communication scheme, probe/substrate pretreatment, probe positioning algorithm, and postimaging data processing procedures that underlie the overall control scheme illustrated in Fig. 3.

1. Software and communication scheme

All positioners are controlled using the provided APT™ (Advanced Positioning Technology) software. Within the APT software, ActiveX controls can be used within LabVIEW (NI LabVIEW 2017 32-bit) to control the positioners. The 700E CH Instruments, Inc., bipotentiostat used throughout this study comes with software that controls all potentiostat functions and measures and records data. The CH Instruments, Inc., software also allows it to interface with LabVIEW such that LabVIEW can be used to simultaneously control both the bipotentiostat and motorized stages. Within LabVIEW, programs are run through virtual instrument (VI) files. The LabVIEW user interface contains graphical representations of functions that are added as nodes and connected to control the flow and sequence of commands. The nodes are graphical objects in LabVIEW that have inputs and/or outputs and perform specific

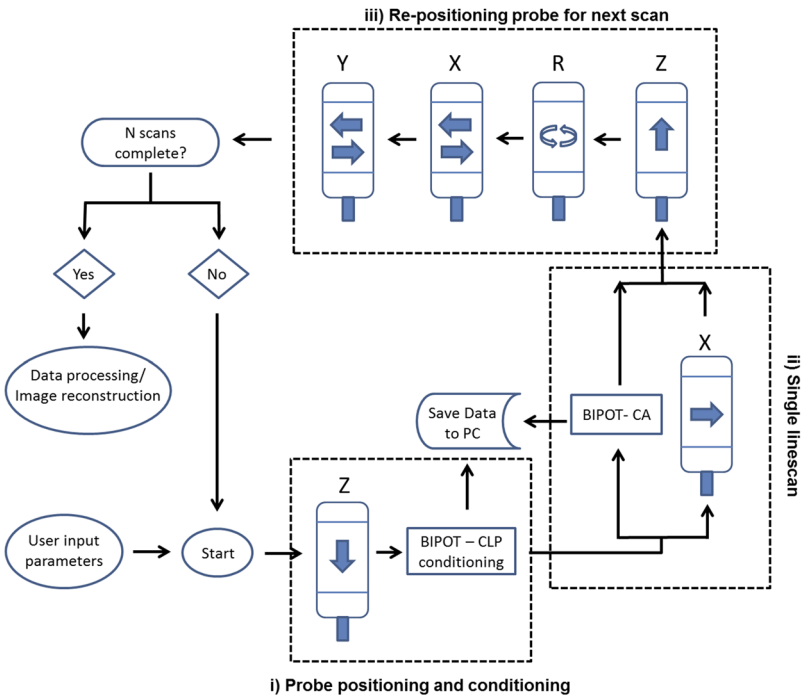

FIG. 3. Process control flow diagram for CLP-SECM imaging. The blocks labeled X, Y, Z, and R represent the microscope positioners, and N represents the total number of scans.

operations when a program runs. Within these objects, the operator specifies the aforementioned user inputs. The authors are happy to provide the LABVIEW code upon request.

2. Electrode preconditioning and vertical positioning of CLP

Some preliminary positional inputs are necessary before a line scan can begin. These include the initial X, Y, and rotational center coordinates as well as the CLP's Z-position. The desired Z position is determined from an approach curve, which is performed by recording the probe signal as the CLP is lowered with the vertical positioner until it comes in contact with the substrate surface. The procedure is very similar to that used in setting up a constant height image acquisition using a conventional SECM instrument. Once all of the necessary initial positional user inputs are stored, the program begins with the vertical positioner lowering the CLP until it is in contact with the substrate. A cyclic voltammetry measurement of the probe surface while it is in contact with the sample surface is taken and the data are saved to the PC. Conditioning of the substrate with a cyclic voltammetry measurement is also done. This preconditioning step is done to "clean" both the probe and substrate surface by oxidizing the organic matter that may be present and clearing the surface of any remaining reactant species from the previous scans. The preconditioning step is important for maintaining a consistent background signal for all scans.

3. Execution of a single CLP line scan

Before a line scan is carried out, the sample stage must be positioned such that (i) the center of the sample area to be imaged is aligned with the midpoint of the CLP, (ii) the distance from the CLP midpoint to the center of the imaging area is set to half of the desired scan length, and (iii) the sample has the proper rotational orientation with respect to the X-scan direction such that the CLP scan will occur at the user-specified scan angle θ_S. After lowering the CLP using the Z-positioner, the line scan measurement begins by initiating potentiostatic control of the substrate and CLP potential, during which the CLP and substrate currents are measured as a function of time. Current measured during these chronoamperometry (CA) measurements is recorded after an initial hold time, typically 240 s, which allows for dampening of transient signals from the CLP and/or substrate before imaging starts. Next, the CA data for the CLP are recorded and saved to the PC while the X-positioner is used to move the sample stage at the user specified step size and dwell time over the user specified scan distance.

4. Sample repositioning between successive scans

Once a line scan finishes, the Z-positioner lifts the CLP off of the substrate and the sample stage must be repositioned for the next scan to be measured at a new scan angle θ_s. Figures 4(a)–4(c) illustrate the procedure used for repositioning the sample stage between scans. After the stage is rotated [Fig. 4(b)] by the user-specified angle θ_s with respect to the rotational center (x_r, y_r), the stage then translates in the X-Y plane with the probe position remaining fixed in the X-Y coordinate system. For every substrate position (x, y), its newly translated position $T(x, y)$ is calculated by assigning the location of the rotational center (x_r, y_r) of the stage and its rotational angle θ_s at the current scan, using the following equation:

$$T(x,y) = \begin{pmatrix} \cos\theta_s - 1 & \sin\theta_s \\ -\sin\theta_s & \cos\theta_s - 1 \end{pmatrix} \begin{pmatrix} x_r \\ y_r \end{pmatrix} + \begin{pmatrix} x \\ y \end{pmatrix}. \quad (2)$$

The translation automatically relocates the substrate back to the scanning area A_{N+1}, which is equal to the initial scanning area A_1 [Fig. 4(c)]. The translation scheme allows us to perform a sequence of CLP scans without the need to position the stage rotational center right at the center of the substrate. This is important since the center of the area to be imaged can be located far from the axis of rotation for the rotational stage. The overall translation scheme is shown pictorially in Fig. 4. Accurate translation of the stage between scans can be ensured as long as the (i) location of the rotation center of the stage (x_r, y_r) relative to the bottom end of the probe is known and (ii) all the reactive species reside within the inscribed circle of scanning area A_1. A more detailed description of this positioning algorithm is presented in Sec. II of the supplementary material.

5. Post-imaging data processing

Electrochemical data acquired by the bipotentiostat are saved as a technical data measurement (.tdm) file with a designated file name and location that is specified by the user at the beginning of the

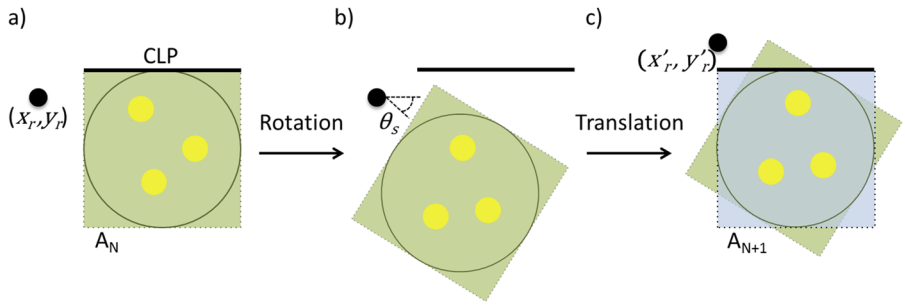

FIG. 4. Schematic top views of the CLP and hypothetical sample containing 3 electroactive disks illustrating how the sample orientation and positioning changes while rotating and translating the stage in between line scans of different scanning angles. (a) The scanning area of the previous scan $\boldsymbol{A_N}$ is shaded in green, while the axis of rotation is located at $(\boldsymbol{x_r}, \boldsymbol{y_r})$ and marked with a dot. (b) View of the CLP and sample after the stage is rotated with respect to $(\boldsymbol{x_r}, \boldsymbol{y_r})$ by an angle θ_s. (c) View of the CLP and sample after translation of the sample stage by the X- and Y-motors to a new position corresponding to the start location for the next scan. The scan area, $\boldsymbol{A_{N+1}}$, for the next scan is shaded gray, while the black circle marks the common area of analysis for both scan angles, which contains all of the electroactive objects of interest.

program run. The saved data can then be opened in a variety of programs (i.e., MATLAB, Excel) for postprocessing with compressed sensing (CS). As detailed in the supplementary material and our previous publication,[22] CS is used to reconstruct 2D SECM images from the current vs distance data acquired during each CLP scan. An abbreviated description of the CS reconstruction procedure used for the exemplary measurements included in this article is also included in the supplementary material.

III. EXEMPLARY CLP-SECM MEASUREMENTS

A. Materials

All electrochemical measurements were carried out in aqueous solutions prepared from 18.2 MΩ-cm deionized water. Concentrated sulfuric acid (Certified ACS plus, Fischer Scientific), sodium sulfate (ACS reagent grade, Sigma Aldrich), potassium hexacyanoferrate(II) trihydrate (ACS reagent grade, Sigma Aldrich), and sodium chloride (ACS reagent grade, Sigma Aldrich) were used as received without further purification. Platinum wire (Alfa Aesar, 99.95% metals basis, 50 μm diameter) served as the counterelectrode while a miniature Ag/AgCl electrode (EDAQ, 3 M KCl) was used as the reference electrode.

1. Fabrication of CLPs

Band microelectrodes were fabricated in a similar manner to what was described by Wehmeyer *et al.*[24] A polycarbonate sheet (TapPlastics, 0.02 in. ≈ 500 μm thick), Pt foil (Alfa Aesar, 99.999% purity), and Kapton tape (1 Mil, 1⁄2″ × 36 yds, Uline) were used as the materials of construction for the CLP. First, the 25 μm thick Pt foil (Fischer Scientific, 99.99% metals basis) was sealed to an insulating polycarbonate substrate using a two-part 5-min epoxy (JB Weld). In order to ensure a good seal between the Pt and the PC substrate, a vice was used to apply uniform pressure overnight while the epoxy cured. The top surface of the Pt foil was electrically insulated using the Kapton tape (thickness ≈70 μm). The thickness of the Kapton tape is very important because it serves as the insulating layer that is in contact with the substrate during measurements and therefore determined the average separation distance between the substrate and Pt layer. The CLP was cut to dimensions of 4.75 mm × 15 mm. The edge of the CLP was exposed by polishing with a home-built polishing system employing 1 μm alumina lapping paper (McMaster-Carr), followed by 0.3 μm alumina slurries. The end of the CLP was polished before measurements using a slurry of 0.05 μm gamma alumina powder on a microcloth polishing pad (CHI Instruments). Cyclic voltammetry (CV) characterization of the CLP in 1.4 mM potassium ferricyanide (ACS Reagant grade, Sigma Aldrich) shows that the CLP exhibits diffusion controlled current at slow scan rates (Fig. S1 of the supplementary material), with a limiting current consistent with that expected for a band electrode with t_E = 25 μm.[26]

2. Fabrication of ultramicroelectrodes (UMEs)

The UMEs used in this study were conventional disk-shaped ultramicroelectrodes made by sealing platinum wires in quartz glass capillaries using a laser-based pipette pulling procedure.[28,29] Platinum microwires (25 μm diameter, Alfa-Aesar) approximately 3 cm in length were attached to the Cu leads (McMaster-Carr, 0.2 mm diameter) using silver epoxy (EpoTek H-22) and subsequently placed into quartz glass capillaries (Sutter Q100-50-10; OD 1 mm, I.D. 0.5 mm). The platinum was sealed in glass after connecting vacuum lines to the open ends of the capillary using Teflon tubing. Two stoppers were placed between the puller bars and the frame in order to minimize the movement of the assembly with respect to the laser. A sealing program (heat: 660; fil: 5; vel: 60; del: 140; pul: 0) was run on average 5–7 times to seal the Pt in glass. After sealing, the stoppers and the vacuum lines were removed and a hard-pull was accomplished using the following program: heat: 875; fil: 2; vel: 120; del: 150; pul: 200. The UMEs were then checked under the microscope to ensure that there were no fractures in the platinum and then polished to 20 μm diameter with a home-built polishing station in order to expose the Pt disk.

3. Fabrication of substrates

The disk electrode patterns were prepared by evaporating metals (Ti as an adhesion layer and Pt as the electrocatalyst) onto degenerately doped p + Si wafers through a shadow mask via electron beam deposition (High Vacuum Angstrom EvoVac, 1×10^{-8} Torr base pressure). Titanium and Pt were deposited sequentially without having to break vacuum. The thicknesses of the Ti and Pt layers were set to 2 nm and 50 nm, respectively. Layer thickness was monitored during the deposition using a quartz crystal thickness monitor. Electrical connection to the back of the p + Si was made by use of silver (Ag) conductive paint (SPI supplies). When the substrate is clamped into the electrochemical cell for imaging, the sample back contact is physically pressed into a piece of copper foil tape (3M Copper Conductive Tapes) placed on the base of the cell. The electrical leads from the potentiostat cable are then attached to the Cu tape.

B. Evaluating uniformity of CLP sensitivity and probe/substrate separation distance

In order for SECM imaging with the CLPs to be reliable and quantitative, it is essential to know if there is any variation in the sensitivity of the probe along its length. Nonuniform sensitivity along the length of the probe can arise from variation in (i) probe/substrate separation along the length of the probe and/or (ii) the intrinsic electrochemical properties in the active sensing element along its length. The sensitivity of the CLP as a function of the probe length can be evaluated by scanning the CLP over a single, isolated electroactive object multiple times such that the object intersects the CLP scan path at different points along the probe. The point of intersection of the disk with the CLP sensing element can be characterized by its distance from the center point of the CLP, w, as shown in the schematic top view of a CLP scan in Fig. 5(a). The CLP used in this study was characterized in an electrolyte of 1 mM H_2SO_4 in 0.1 M Na_2SO_4 by scanning it at 25 μm s^{-1} over an isolated 100 μm diameter Pt disk electrode for 13 different w. The measurement was carried out in the substrate generation/probe collection mode, resulting in positive feedback from the H_2/H^+ redox reactions occurring between the disk electrode and the sensing element of the probe.

Using the peak current recorded by the probe during each scan as a proxy for the probe sensitivity, the probe sensitivity is plotted as a function of w in Fig. 5(b). For CLP scans characterized by w greater

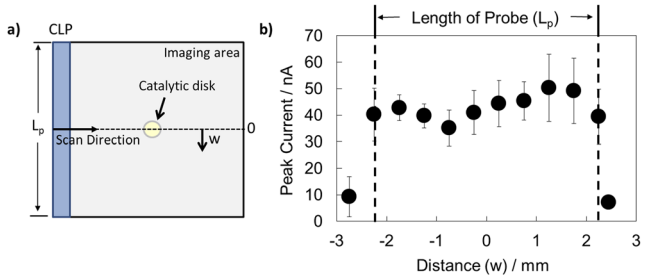

FIG. 5. (a) Schematic showing the characterization procedure of the CLP as it scans over a single electroactive disk with a diameter of 100 μm at various locations along the length of the probe (w). (b) Plot of the peak current measured from the CLP as a function of w. The error bars correspond to the 95% confidence interval for the average peak current density recorded during three different CLP scans at each location. The measurements were carried out in the substrate generation probe collection mode in 1 mM H_2SO_4 in 0.1 M Na_2SO_4 at a scan rate of 25 μm s^{-1}. The CLP potential was held at 0.7 V vs Ag|AgCl, and the sample was held at −0.8 V vs Ag|AgCl.

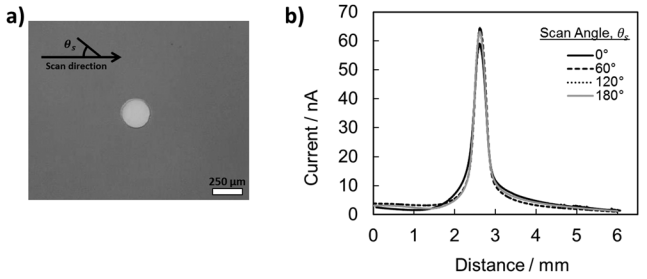

FIG. 6. (a) An optical image of a platinum disk with a diameter of 250 μm. (b) CLP line scans over the disk electrode (a), recorded at varying scan angles at a step size of 10 μm s^{-1} in 1 mM H_2SO_4 and 0.1 M Na_2SO_4. The CLP potential was held at 0.7 V vs Ag|AgCl, and the substrate was held at a mass transfer limiting potential for the hydrogen evolution reaction at −0.8 V vs Ag|AgCl.

than half the length of the CLP ($L_p/2$), ($w = -2.75$ mm, +2.45 mm), a negligible signal is recorded because the CLP scan path does not intersect the electroactive disk. When w < ($L_p/2$), a significant peak current is observed, with an average signal of 37 ± 4 nA recorded. Slight variations in probe sensitivity can be seen, including a minimum around $w = -1$ mm. Such nonuniformities might arise due to small inconsistencies in the cleanliness of the edge of the platinum foil sensing element, which might be caused by nonuniform polishing treatment and/or small amounts of residual organic matter that were not effectively removed during CV conditioning. Minor "edge effects," where the peak current is slightly reduced for $w \approx \pm(L_p/2)$, are also visible. A subtle increase in the recorded peak current with increasing w is also present, which can result from the end of the CLP not being perfectly parallel with the sample surface. The measurements in Fig. 5(b) highlight the importance of taking great care to (i) fabricate well-defined CLP probes and (ii) position the CLP flush on the sample surface. Accurate CS-reconstruction of an SECM image does not require perfectly uniform sensitivity along the length of the CLP, but it is important to characterize nonuniformities in instances where significant variation in probe sensitivity exists. As we will detail in a future communication, CS reconstruction algorithms can use the probe sensitivity profile, such as that shown in Fig. 5, to filter out artifacts of probe nonuniformities from the final reconstructed image.

C. Validating the CLP positioning algorithm

To validate the accuracy of the positioning algorithm described in Sec. II of the supplementary material, CLP line scans were conducted over a single 250 μm diameter electroactive Pt disk (Fig. 6) at four different scan angles, θ_s. The scans were recorded using the same conditions used for the CLP line scan measurements in Fig. 5(b), except that a slower scan rate of 10 μm s^{-1} was employed. As desired, the CLP line scan profiles at each of the four scan angles overlay almost exactly [Fig. 6(b)], confirming that our positioning algorithm accurately rotates and translates the stage in between scans such that the CLP and electroactive disk intersect each other at the midpoint of the scan. This feature is not needed if the center of the imaging region of interest corresponds exactly to the rotational center of the stage but is critically important when those two points are not the same. Some slight variation in the peak current is seen for the four different CLP scan angles in Fig. 6(b), which might be explained by the small differences in sensitivity along the length of the probe that were shown in Fig. 5(b).

D. Demonstration of CLP-SECM imaging

Having characterized the CLP sensitivity profile and validated the substrate positioning algorithm, a demonstration of CLP-SECM imaging was carried out using a sample containing three electroactive Pt disks with diameters of 150 μm [Fig. 7(a)]. Seven total CLP line scans were recorded sequentially using the process control scheme shown in Fig. 3 and using the identical scan conditions described for the line scan measurements shown in Fig. 6. The raw line scan signal for each of the scans is provided in Fig. 7(b). These data were then fed to the compressed sensing (CS) postprocessing code for image reconstruction to produce the 2D CLP-SECM image located in Fig. 7(c). A detailed description of the CS reconstruction algorithm can be found in our prior publication,[22] while details specific to its implementation in this work are provided in Sec. III of the supplementary material.

The CS-reconstructed CLP-SECM image in Fig. 7(c) accurately displays three circular features having diameters and locations that are in good agreement with the location of the disk electrodes shown in Fig. 7(a). Four scans were used to generate the reconstructed image in Fig. 7(c), but as few as 3 scans were found to be sufficient to accurately determine that three-disk electrodes were present on the surface. Figure S3 of the supplementary material shows how the quality of the reconstructed image of the 3-disk sample changes when using 3, 4, 5, and 6 line scans. As expected for identical disk electrodes, the three disks displayed in the reconstructed image all exhibit similar signal intensity. For comparison, SECM imaging of the same sample was carried out using a conventional UME with a commercial CHI 700E SECM instrument, with the result shown in Fig. 7(d). A ≈20 μm diameter Pt UME, similar to the thickness of the Pt foil used for the electroactive layer in the CLP (≈25 μm), was used for the conventional SECM measurement. Imaging with the UME was performed using a probe/substrate separation

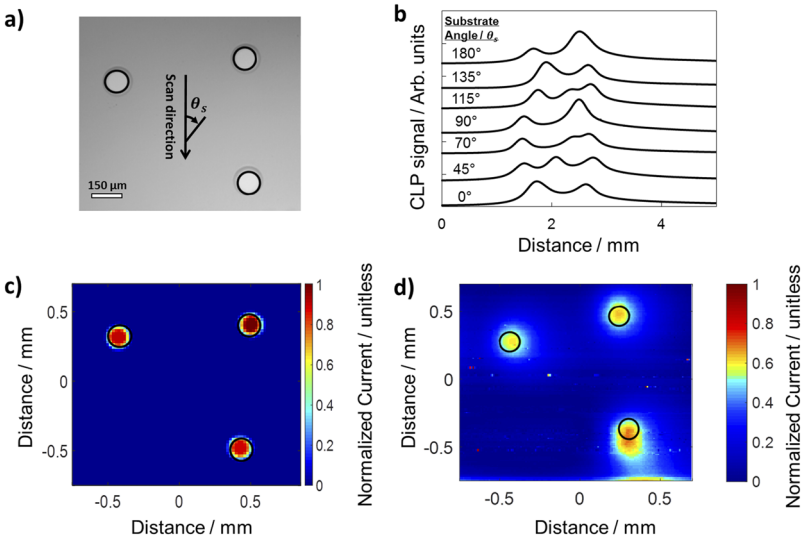

FIG. 7. (a) Optical image of a sample consisting of three platinum disks deposited onto an inert p + Si substrate. The arrow that is superimposed on this image indicates the CLP scanning direction, while the stage is rotating clockwise by an angle θ_s. (b) Individual CLP scans recorded for seven different sample rotation angles. (c) SECM image reconstructed from 4 of the line scans (0°, 45°, 70°, and 135°) shown in panel (b) using compressed sensing. (d) SECM image generated by a conventional SECM instrument using a UME characterized by a probe diameter of ≈20 μm. All SECM measurements were carried out in substrate-generation, probe collection mode in a solution of 1 mM H_2SO_4 in 0.1 M Na_2SO_4 using a probe scan rate of 10 μm s^{-1}, a probe potential of 0.7 V vs Ag|AgCl, and a substrate potential of −0.8 V vs Ag|AgCl. The superimposed black circles in panels (c) and (d) are used to show the physical size and relative locations of the three Pt disks compared to the features recorded in the SECM measurements. The conventional SECM image was recorded by scanning the probe from left to right, starting at the top of the sample area and working downwards in a raster pattern.

distance of 60 μm, identical to the average probe/substrate separation distance for the CLP when it is positioned at an angle of θ_{CLP} = 45° with respect to the substrate surface. In comparing the SECM images shown in Figs. 7(c) and 7(d), we find that the use of CLPs and UMEs with similar probe critical dimensions, probe/substrate separation distance, and identical scan rates (10 μm s^{-1}) results in SECM images of similar quality. However, there is some distortion in the point-probe SECM image at the end of the scan, most likely due to sample drift and/or changes in the electrochemical environment from evaporation of the electrolyte over the long measurement period. Although the conventional SECM image has similar quality than the CLP-SECM image, the former required ≈9 h of imaging compared to the ≈1 h of scan time required to complete the 4 CLP line scans used to reconstruct the latter. It should also be noted that this large time advantage was achieved while scanning over a circular sample area that was roughly two times larger than the rectangular area imaged by the UME. As detailed in our first publication on CLP-SECM,[22] the total imaging time required for imaging with nonlocal probes can be orders of magnitude less than a conventional UME for samples that are characterized by even larger ratios of the scan area dimension to the desired imaging resolution.

IV. CONCLUSIONS

This article described the design, operating principles, and implementation of a programmable scanning electrochemical microscope that allows for high-throughput imaging with nonlocal continuous line probes. The key novelty of this instrument compared to commercial SECM instruments is that it possesses a programmable rotational sample stage that allows for automated imaging with a CLP at scan angles from 0° to 360°. In addition to describing the overall design and control scheme for the microscope, this article presented methods for CLP characterization and validation of the probe positioning algorithm. A side-by-side imaging comparison of CLP-SECM with the conventional SECM was also carried out using a sample based on three Pt disk electrodes. This comparison shows that a CLP-SECM instrument is capable of generating CS-reconstructed SECM images with similar quality to those generated with a commercial SECM instrument using a conventional UME probe of similar critical dimension and probe/substrate separation distance. Overall, this result demonstrates the potential of SECM instruments employing nonlocal probes such as CLPs to drastically reduce SECM imaging rates compared to conventional SECMs based on UME "point probes."

SUPPLEMENTARY MATERIAL

See the supplementary material for more information on CLP characterization, the automated sample alignment procedure, and a more detailed description of CS and the image reconstruction algorithm.

ACKNOWLEDGMENTS

The authors would like to acknowledge funding support from the National Science Foundation under Grant No. NSF CHE-1710400. Any opinions, findings, and conclusions or recommendations expressed in this material are those of the author(s) and do not necessarily reflect the views of the National Science Foundation. The authors would also like to acknowledge Adekunle David Balogun for helping with fabricating electrochemical cell prototypes.

REFERENCES

[1]C. L. Bentley, J. Edmondson, G. N. Meloni, D. Perry, V. Shkirskiy, and P. R. Unwin, Anal. Chem. **91**, 84 (2018).
[2]T. H. Muster, A. Trinchi, T. A. Markley, D. Lau, P. Martin, A. Bradbury, A. Bendavid, and S. Dligatch, Electrochim. Acta **56**, 9679 (2011).
[3]S. Amemiya, A. J. Bard, F.-R. F. Fan, M. V. Mirkin, and P. R. Unwin, Annu. Rev. Anal. Chem. **1**, 95 (2008).
[4]M. V. Mirkin, W. Nogala, J. Velmurugan, and Y. Wang, Phys. Chem. Chem. Phys. **13**, 21196 (2011).

[5]P. Sun, F. O. Laforge, and M. V. Mirkin, Phys. Chem. Chem. Phys. **9**, 802 (2007).
[6]O. E. Hüsser, J. Electrochem. Soc. **136**, 3222 (1989).
[7]C. G. Zoski, J. Electrochem. Soc. **163**, H3088 (2016).
[8]Y. Takahashi, A. I. Shevchuk, P. Novak, Y. Murakami, H. Shiku, Y. E. Korchev, and T. Matsue, J. Am. Chem. Soc. **132**, 10118 (2010).
[9]B. Gollas, P. N. Bartlett, and G. Denuault, Anal. Chem. **72**, 349 (2000).
[10]T. H. Treutler and G. Wittstock, Electrochim. Acta **48**, 2923 (2003).
[11]J. Romberg, IEEE Signal Process. Mag. **25**(2), 14–20 (2008).
[12]R. J. Fasching, Y. Tao, and F. B. Prinz, Sens. Actuators, B **108**, 964 (2005).
[13]A. Lesch, D. Momotenko, F. Cortés-Salazar, I. Wirth, U. M. Tefashe, F. Meiners, B. Vaske, H. H. Girault, and G. Wittstock, J. Electroanal. Chem. **666**, 52 (2012).
[14]A. Lesch, D. Momotenko, F. Cortés-Salazar, F. Roelfs, H. H. Girault, and G. Wittstock, Electrochim. Acta **110**, 30 (2013).
[15]M. P. Nagale and I. Fritsch, Anal. Chem. **70**, 2902 (1998).
[16]D. J. Comstock, J. W. Elam, M. J. Pellin, and M. C. Hersam, Anal. Chem. **82**, 1270 (2010).
[17]E. J. Candes and M. B. Wakin, IEEE Signal Process. Mag. **25**, 21 (2008).
[18]M. A. Davenport, M. F. Duarte, Y. C. Eldar, and G. Kutyniok, *Compressed Sensing: Theory and Applications* (IEEE Signal Processing Magazine, 2009), p. 1.
[19]D. Momotenko, J. C. Byers, K. McKelvey, M. Kang, and P. R. Unwin, ACS Nano **9**, 8942 (2015).
[20]B. D. B. Aaronson, J. C. Byers, A. W. Colburn, K. McKelvey, and P. R. Unwin, Anal. Chem. **87**, 4129 (2015).
[21]J. M. Gregoire, C. Xiang, X. Liu, M. Marcin, and J. Jin, Rev. Sci. Instrum. **84**, 024102 (2013).
[22]G. D. O'Neil, H. W. Kuo, D. N. Lomax, J. Wright, and D. V. Esposito, Anal. Chem. **90**, 11531 (2018).
[23]D. V. Esposito, J. B. Baxter, J. John, N. S. Lewis, T. P. Moffat, T. Ogitsu, G. D. O'Neil, T. A. Pham, A. A. Talin, J. M. Velazquez, and B. C. Wood, Energy Environ. Sci. **8**, 2863 (2015).
[24]K. R. Wehmeyer, M. R. Deakin, and R. M. Wightman, Anal. Chem. **57**, 1913 (1985).
[25]A. Lesch, B. Vaske, F. Meiners, D. Momotenko, F. Cortés-Salazar, H. H. Girault, and G. Wittstock, Angew. Chem., Int. Ed. **51**, 10413 (2012).
[26]A. J. Bard and L. R. Faulkner, *Electrochemical Methods Fundamentals and Applications*, 2nd ed. (Wiley, 2001).
[27]J. Kwak and A. J. Bard, Anal. Chem. **61**, 1221 (1989).
[28]M. A. Mezour, M. Morin, and J. Mauzeroll, Anal. Chem. **83**, 2378 (2011).
[29]T. J. Cardwell, J. Mocak, J. H. Santos, and A. M. Bond, Analyst **121**, 357 (1996).